Alkane Trapping onto Structured Alkane Monolayers on Pt(111) at Low Temperature

A. F. Carlsson and R. J. Madix*

Department of Chemical Engineering Stanford University, Stanford, California 94305

Received: May 2, 2000; In Final Form: September 26, 2000

The trapping dynamics of methane and ethane onto preadsorbed methane-, ethane-, propane-, and *n*-butane-saturated layers on Pt(111) at 30 and 50 K have been investigated using supersonic molecular beam techniques. At these low temperatures, multilayers of the incident molecule continue to build without the complication of desorption, and the weakly bound extrinsic precursor state is stabilized. The initial trapping of ethane into the extrinsic precursor state is enhanced to the same degree on all the covered surfaces compared to trapping on the clean surface, but the initial trapping probability of methane, though enhanced by the adlayers, is more complex. The trapping probability of CH_4 increases toward unity on all these surfaces as methane adsorbs and levels off at 0.96, independent of the type of adsorbate covering the bare surface. The angular dependence of the initial trapping probability indicates an increasing corrugation in the CH_4−surface potential with increasing chain length of adsorbate; for comparison, methane traps on the clean surface with normal energy scaling,[1] whereas it traps on the *n*-butane-covered surface with near-total energy scaling.

Introduction

Most industrial heterogeneous catalysis occurs under conditions where the surface may be partially or fully covered with adsorbates, which may compete for adsorption sites and facilitate or hinder the adsorption of gas-phase molecules. An understanding of molecular adsorption on clean and partially covered surfaces of transition metals is important to engineering heterogeneous catalysis, crystal growth, thin film growth, and lubrication processes.[2] Atomic and molecular adsorption on clean surfaces has been well studied,[3−6] but only recently has consideration been given to adsorption on adsorbate-covered surfaces.[7−11]

The energy of the incident molecule must be accommodated by the surface or adsorbed species through a combination of energy dissipation to lattice phonons and to the adsorbed molecules. Adsorbed molecules may serve as a route to an extrinsic precursor[12] to molecular adsorption by facilitating trapping by dissipating or redirecting the translational energy of the incoming molecule. Species physisorbed in a second layer which may act as extrinsic precursors have been isolated at low temperatures[13−24] and identified spectroscopically.[17−25] The presence of extrinsic[26−37] and intrinsic[34−37] precursors has also been deduced from molecular beam studies. Intrinsic precursors have been deduced from thermal programmed desorption and isotope experiments and spectroscopic measurements.[38−40] Intrinsic precursors are usually invoked in mechanisms for chemisorption, where a weakly adsorbed molecular state is a precursor to dissociation or to a strongly bound state. In the case of molecular (physical) adsorption, it makes little sense to speak of a thermally equilibrated intrinsic precursor because a molecule that has trapped and is thermally equilibrated with the surface is molecularly adsorbed, even though it may be mobile. Thus, only the extrinsic precursor state is relevant to this study of weak molecular adsorption.

The trapping probability into a precursor state is approximately independent of temperature.[2] Thus, trapping into the extrinsic precursor state may occur at a temperature above which this weakly adsorbed state is stable, and the molecule can either migrate to a bare metal surface site or desorb. In this study, we probe molecular adsorption into the extrinsic precursor state by holding the surface at temperatures well below the desorption temperature from multilayers, thus avoiding complications arising from competitive desorption of the precursor.

Generally, the modified Kisliuk model describes the coverage dependence of the molecular adsorption probability.[1,41,42] It has been used to describe the coverage-dependent trapping probabilities of ethane,[41] methane,[1] and argon[42] on Pt(111). Assuming that the adsorbed molecules do not interact with each other and that adsorption into the final state is irreversible, we may represent the modified Kisliuk modelas[41,43] the following, where A(g) is the gas-phase species, A′ is the extrinsic precursor, A(a) is the final adsorbed species, F is the incident flux in monolayers/sec, S_o' is the initial adsorption probability into the extrinsic precursor, and S_o is the initial adsorption probability directly onto the binding site:

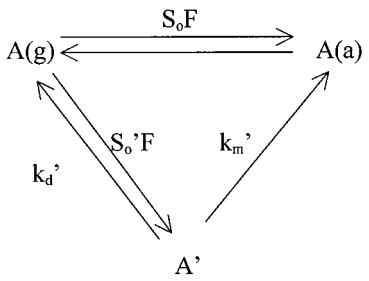

Assuming a steady-state concentration of the extrinsic precursor gives

$$S(\theta) = S_o(1-\theta) + \frac{S_o'(1-\theta)q_m\theta}{(1-q_m\theta)}$$

10.1021/jp001655p CCC: $19.00
Published on Web 12/06/2000

where

$$q_m = \frac{k_m'}{k_d' + k_m'}$$

As long as the ratio of rate constants q_m is near but less than unity and $S_o' > S_o$, the adsorption probability will increase as the coverage is increased to near 1 ML, where the adsorption probability will rapidly fall to zero. Typically, the value of S_o' required to fit the coverage dependence of $S(\theta)$ is 5% to 10% higher than the value measured directly by the King and Wells pressure drop at saturation coverage, due to competitive desorption from the precursor state.[1,41,42] In this study, we have investigated trapping probabilities onto precovered surfaces where the second layer is stable to isolate the dynamics of molecular trapping into the extrinsic precursor state.

The dependence of the molecular trapping into an extrinsic precursor state on incident angle and/or energy may be different for adsorbate-covered surfaces of methane, ethane, propane, and *n*-butane on Pt(111) due to the different masses and surface structures. For the best definition of the gas−surface potential, overlayers with defined coverages and structures should be employed. Firment and Somorjai[44] have identified ordered structures of C_4-C_8 alkanes with LEED, but they were not able to cool methane, ethane, and propane to a low enough temperature ($T < 90$ K) to stabilize the structures. Nonetheless, their studies suggest that ordered structures of these species should exist. Temperatures well below the desorption temperature of these species are needed in order to observe LEED patterns due to local heating of the surface by the impinging electrons which cause desorption of the surface species. The LEED experiments are further complicated because the LEED electrons dissociate a small fraction of molecules on the surface, as shown by AES after such an experiment. LEED results for C_1-C_4 alkanes are presented below.

It is also interesting to compare the effects of weakly bound molecules from trapping to the differences produced by rigidly bound species. Ethane trapping on rigid adsorbate-covered surfaces such as Pt(111)−S[8] and Pt(111)−O[9] has been shown to exhibit total energy scaling. Using molecular dynamics simulations, Stinnett and Madix[8] showed that corrugation in the gas−surface potential facilitates the conversion of perpendicular to parallel momentum at normal incidence but backscatters molecules at glancing incidence. These principles may or may not apply to less rigid adsorbates such as methane, ethane, propane, or butane, which have a different gas−surface potential and which may be more easily displaced on the surface than the rigidly bound adsorbates—though simulations of argon trapping on argon-covered surfaces by Head-Gordon and Tully suggest that static corrugation does play an important role.[7] Comparisons of ethane trapping on sulfur- and oxygen-covered Pt(111)[8,9] indicate that the trapping probability is approximately independent of the adsorbate mass, contrary to what is suggested by the Baule formula,[45] hard cube models,[46−49] and soft cube models.[13] For example, at normal incidence and 10 kJ/mol, the trapping probability of ethane is 0.85 on the S-covered surface and 0.81 on the O-covered surface; at 30 kJ/mol, the trapping probability of ethane is 0.85 on the S-covered surface and 0.81 on the O-covered surface. In fact, both S and O only serve to increase the potential corrugation and to transfer energy to lattice vibration. The metal−adsorbate vibration itself is not excited by collision.[8,9]

In this molecular beam study, we present initial trapping probabilities for methane and ethane incident upon a series of molecularly adsorbed alkanes in ordered structures at temperatures low enough to stabilize the second adsorbed layer for each system. Initial trapping probability measurements were taken at 31 and 50 K for methane and ethane, respectively. These experiments determine the dynamics of molecular trapping into the extrinsic precursor state and allow the elucidation of adsorbate effects on molecular trapping.

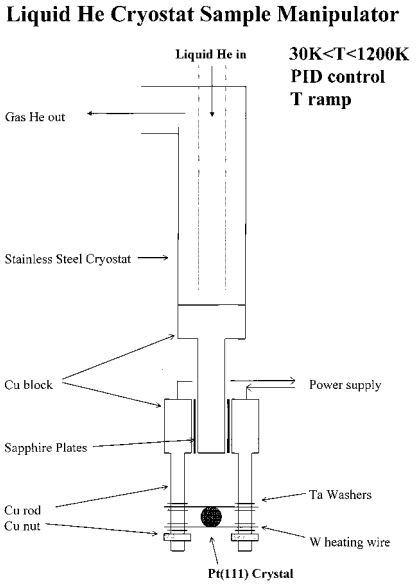

Figure 1. Liquid He cryostat sample manipulator.

Experimental Section

The experimental apparatus used in this study has been described in detail elsewhere.[50] It consists of an ultrahigh vacuum chamber with a base pressure of 5×10^{-11} Torr coupled to a triply pumped supersonic molecular beam source. The main chamber is equipped with a rear view LEED/AES electron optics and two quadrupole mass spectrometers. The first mass spectrometer is mounted on a bellow and has a flow through the Fuelner cap[51,52] on the ionizer; the hole in the cap can be placed 1 mm in front of the sample for selective detection of components desorbing from the surface. The second mass spectrometer can be rotated 180° about the sample at a fixed radius of 10.5 cm and is used in conjunction with a lock-in amplifier and 50% duty beam chopper to measure the velocity of the molecules in the beam. The Pt(111) crystal (10 mm diameter) was cleaned by cycles of Ar^+ sputtering and oxygen cleaning, although typically only one cycle of oxygen cleaning was needed each day. When surface impurity concentrations were below the sensitivity of AES (<0.01 ML) and a sharp p(1 × 1) hexagonal LEED pattern was observed, the surface was assumed to be clean and well-ordered.

The molecular beam is formed by the supersonic expansion of gas through a monel nozzle that can be heated resistively with proportional-integral-derivative (PID) control to 750 K. The flux of molecules at the crystal is about 10^{14}/s on a 0.07 cm^2 spot. Low-energy beams (10kJ/mol) were formed with pure alkanes, whereas high-energy beams were formed by seeding the alkane in helium and heating the nozzle.

The sample can be resistively heated with PID control to 1200 K and cooled to 30 K using a liquid helium cryostat (shown in Figure 1). The stainless steel coldfinger (Janis Research) is gold-plated at the bottom, where it connects to the copper sample holder. Sapphire plates are used in series with tungsten wires to support the sample and heat it resistively while at the same

time isolating it from ground and allowing heat to flow to the coldfinger. We were able to reach a lower limit of 83 K with liquid nitrogen in the coldfinger and 30 K with a constant flow of liquid helium. Temperatures were measured to ±0.5 K using 0.125 mm chromel and alumel thermocouple wires spot-welded to the back of the crystal and braided to 0.5 mm wires of the same type, which run up the manipulator to the feedthrough to minimize offsets in the thermocouple voltage due to thermal gradients.[53] This setup measured 5 K in liquid helium and 77 K in liquid nitrogen, and consequently, no corrections were made to the thermocouple readings. TPD experiments were performed after cooling the sample to 30 K and letting a beam of methane strike the inert flag for the time needed to complete a dynamic trapping probability experiment (DTPE); no m/z = 2, 16, 18, 28, 32, or 44 was detected up to 860 K.

The method of King and Wells[54] was used to measure direct sticking probabilities using a shutter in the beam source chamber and an inert, gold-plated flag in the main chamber. The partial pressure of the alkane in the beam was measured with the stationary mass spectrometer as a function of time. When the shutter and flag were both blocking the beam, a background reference was taken. At 20 s, the shutter was opened, and the background pressure of the beam scattering off the inert flag was measured. At 40 s, the flag was lowered, and the beam was allowed to impinge on the crystal. At our large pumping speeds,[55] the ratio of the drop in the partial pressure of the alkane measured at time t to the partial pressure when it scattered off the inert flag is the net sticking probability on the surface. In particular, initial trapping probabilities were measured with an experimental error of ±0.02 for various incident angles and energies.

The crystal was positioned at angles of 0−60° to the incident beam during trapping probability measurements. It was verified that the entire beam was impinging on the crystal at each position by monitoring a modulated helium beam with the rotatable mass spectrometer placed behind the crystal. At glancing incident angles, the crystal was turned away from the stationary mass spectrometer to avoid direct contributions from scattered components to the sticking probability measurement.

LEED images of methane-, ethane-, and propane-covered surfaces were recorded using an MTI VE1000SIT special low-light video camera and a Panasonic SVHS AG1970 videotape recorder. Due to local heating and some decomposition by the low-energy electrons, the diffraction image was stable for less than 5 s. While the video camera was recording, the sample was moved continuously so that the electron beam continuously hit new surface regions. The images on videotape were then captured and digitized using a Powermac 7100 computer and saved in compressed jpg format. The modified images and digital processing were created with Adobe Photoshop software. During recording, all lights in the laboratory were turned off, the viewports were covered, and a black cover was wrapped around the camera and viewport to the rear view LEED (OCI Vacuum Microengineering). The LEED beam current was 0.2 μA on a 500 μm diameter spot at a beam energy of 38 eV.

Surface coverages were measured using a calibrated leak system[56] consisting of a 426.7 mL stainless steel backing chamber with an MKS Baratron 121A pressure gauge attached to a 10 μm pinhole leak gasket at the entrance to the main chamber. The area of the beam spot on the crystal was calibrated[57] with the well-characterized CO/Pt(111)[58] system and found to be 0.07 cm,^{2} in good agreement with predictions from the beam collimating geometry. The change in pressure of the backing chamber is related to the conductance of the pinhole leak by

$$c = -\frac{1}{P}\frac{\mathrm{d}n}{\mathrm{d}t} = \frac{V}{kT}\frac{d\ln(P/P_o)}{\mathrm{d}t} \tag{1}$$

where c is the conductance, P is the pressure in the backing chamber, n is the number of molecules, t is time, V is the storage volume, k is Boltzmann's constant, and P_o is the initial pressure in the backing chamber. The calibrated conductance was then used to calculate the coverage on the surface during beam exposure using

$$F = \frac{l_b}{A_b} \tag{2}$$

$$\frac{l_b}{l_c} = \frac{V_b}{V_c} \tag{3}$$

$$\theta = \int_0^t FS(t)\,\mathrm{d}t \tag{4}$$

where F is the flux, l_b is the leak rate of the beam, A_b is the area of the beam, l_c is the leak rate of the calibrated leak, V_b is the mass spec voltage due to the beam background, V_c is the mass spec voltage due to the calibrated leak background, $S(t)$ is the net sticking probability as a function of time, and θ is the coverage.

Results

Surface Characterization. *Coverage Calibration.* A calibrated leak system[42,56] was utilized to calibrate the coverage of the ordered structures for each of the alkanes used as adsorbates on the clean Pt(111) surface. Measurements were reproducible within 10%. The coverages were methane (0.237 ML = 0.237 C/Pt), ethane (0.227 ML = 0.45 C/Pt), propane (0.205 ML = 0.61 C/Pt), the low-coverage structure of *n*-butane (0.14 ML = 0.56 C/Pt), and the high-coverage structure of *n*-butane (0.20 ML = 0.80 C/Pt).[57] The conductance of the calibrated leak was determined by following the pressure drop in a fixed backing volume as a function of time using the Baratron gauge. The calibrated conductance for a particular gas was then used to determine the beam flux and the coverage of the species on the surface by using the mass spectrometer signal as a measure of the background pressure of the gas by alternatively using the beam and the calibrated leak as sources of the gas. First, a DTPE of methane (for example) on the clean surface was completed (Figure 2), and directly following that, a fixed pressure of methane in the backing chamber was utilized to leak methane into the chamber at a known rate (Figure 2). The mass spectrometer signal due to methane scattering from the inert flag, V_b, and the mass spectrometer signal due to the known leak rate of methane from the calibrated leak, V_c, were then used to calculate the coverage on the surface using the relationship

$$\theta = CP_c\frac{1}{V_c}\frac{A_v}{A_b}$$

where A_b = 0.071 cm^2, $C = 9.651 \times 10^{13}$ (for methane), and A_v is the shaded area in the top panel of Figure 2 resulting from the integration of the adsorption probability during trapping; the surface density for Pt(111) was taken to be 1.5×10^{15} Pt/cm^3 to convert to units of monolayers.

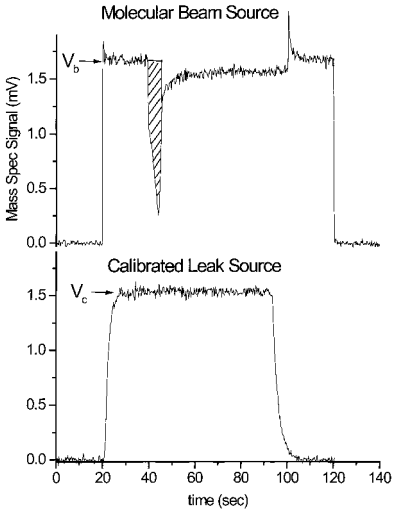

Figure 2. Beam flux determinations using the calibrated leak. The voltage given by the mass spectrometer during a King and Wells experiment (top panel) is compared to the voltage given by letting a known amount of gas in through the calibrated leak (bottom panel) to calculate the amount of gas adsorbed before saturation (shaded area, top panel) during the King and Wells trace.

LEED. The structures of methane, ethane, propane, and *n*-butane on Pt(111) were studied with LEED at low surface temperatures and a beam energy of 38 eV. Higher beam energies made the sharp diffraction features become dim and diffuse, presumably due mostly to local heating of the surface and desorption of the alkane, although some electron-induced dissociation also occurred. Slight carbon contamination was detected by AES after the LEED experiment was finished. Images were taken at a low enough beam energy that the image was stable for 2−5 s, during which the image was recorded.

The traditional definitions[44] of the substrate and adsorbate unit mesh are used to represent the LEED structures. The real-space unit mesh vectors of the adsorbate are defined relative to the substrate as $\mathbf{b_1} = b_{11}\mathbf{a_1} + b_{12}\mathbf{a_2}$ and $\mathbf{b_2} = b_{21}\mathbf{a_1} + b_{22}\mathbf{a_2}$, where $\mathbf{a_1}$ and $\mathbf{a_2}$ are the real-space substrate unit mesh vectors The adsorbate structure is then represented in matrix notation as

$$\begin{vmatrix} b_{11} & b_{12} \\ b_{21} & b_{22} \end{vmatrix}$$

Each of the alkane-covered surfaces was prepared by dosing the alkane at temperatures sufficiently high to prevent multilayer formation but low enough to prevent desorption from the monolayer[59] and subsequently quenching the surface to a temperature below which multilayers form. Low temperatures were needed to minimize surface mobility of the alkanes, which made LEED patterns diffuse or nonexistent at higher temperatures. The observed LEED patterns are complex. Our purpose here is not to determine accurately the real-space structures of the alkanes but to establish that ordered structures do form at known coverages. We thus suggest only plausible real-space structures where possible.

Pt(111)−CH_4. The clean surface was exposed to a background dose of methane at 3×10^{-8} Torr for 2 min at 50 K and subsequently quenched to 31 K in order to produce the LEED pattern shown in Figure 3; the outermost hexagonal spots correspond to the p(1 × 1) structure of Pt(111). The streaked hexagonal pattern of spots is suggestive of a c($\sqrt{3} \times 5$) structure

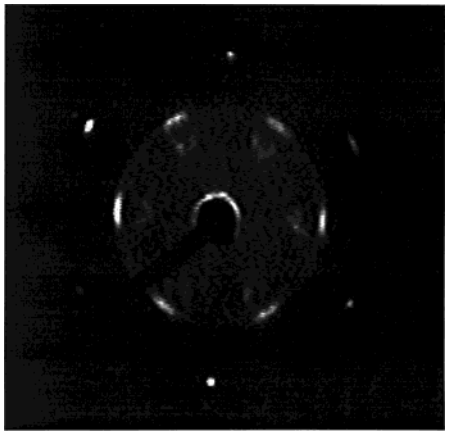

Figure 3. LEED image of Pt(111)−CH_4 at a surface temperature of 30 K and a beam energy of 38 eV.

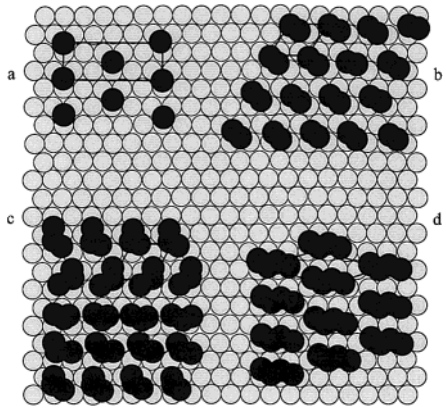

Figure 4. Real-space structures of c($\sqrt{3} \times 5$) CH_4 (a), p(2 × 2) C_2H_6 (b), p(2 × 2) C_3H_8 (c), and *n*-C_4H_{10} (d) on Pt(111) suggested by LEED analysis. Different orientations of propane are shown (c) with an overall p(2 × 2) symmetry.

with three rotational domains, corresponding to a real-space unit cell of

$$\begin{vmatrix} 5 & 0 \\ 3 & 1 \end{vmatrix}$$

and a coverage of 0.20 ML. The coverage calibration of 0.237 ML suggests a compression of this structure or coexistence with a ($\sqrt{3} \times \sqrt{3}$)R30 structure. The c($\sqrt{3} \times 5$) real-space structure is shown in Figure 4a.

Pt(111)−C_2H_6. The clean surface was exposed to a background dose of ethane at 3×10^{-8} Torr for 2 min at 95 K and subsequently quenched to 35 K in order to produce the LEED pattern shown in Figure 5; the outer hexagon of single spots define the substrate p(1 × 1). The inner groups of four spots are suggestive of a p(2 × 2) structure with diffraction features split by antiphase domain boundaries.[60−64] The perfect p(2 × 2) structure has a coverage of 0.25 ML, in good agreement with the coverage calibration of 0.227 ML, considering the possible presence of domain boundaries. The central four split-spots are split with hexagonal symmetry, but the remaining two spots of each set of six (along the "radial" direction) are not.

Each domain can be treated as a scattering center in order to determine the overall spot splitting.[65] Simulation of different antiphase domain superstructures suggests that the domains form superstructures of

$$\begin{vmatrix} 3 & 2 \\ 3 & 0 \end{vmatrix}$$

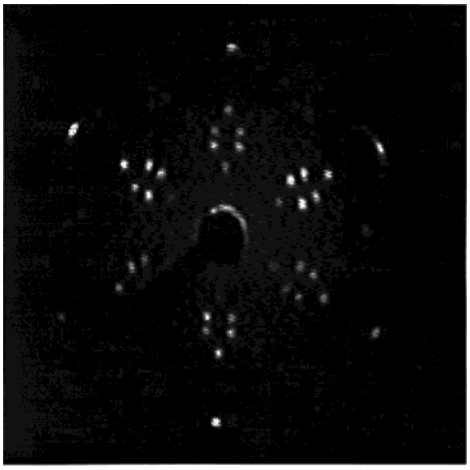

Figure 5. LEED image of Pt(111)−C_2H_6 at a surface temperature of 30 K and a beam energy of 38 eV.

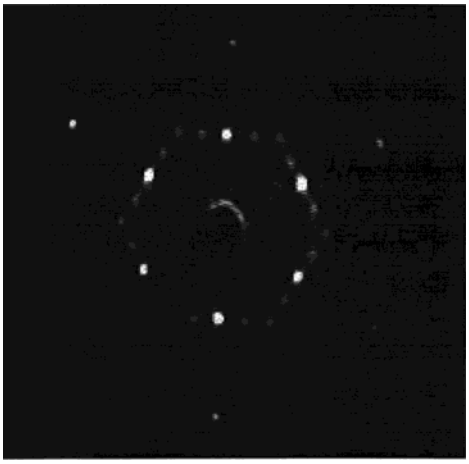

Figure 6. LEED image of Pt(111)−C_3H_8 at a surface temperature of 30 K and a beam energy of 38 eV.

and

$$\begin{vmatrix} 2 & 3 \\ 0 & 3 \end{vmatrix}$$

which are separated by the vectors $(l_1,l_2) = (3,2)$, (3,0), (2,3), and (0,3). The p(2 × 2) structure for Pt(111)−C_2H_6 is shown in Figure 4b.

Pt(111)−C_3H_8. The clean surface was exposed to a background dose of propane at 3×10^{-8} Torr for 2 min at 110 K and subsequently quenched to 35 K in order to produce the LEED pattern shown in Figure 6. The brightest diffraction features are suggestive of a p(2 × 2) structure, while additional less intense spots suggest an antiphase domain splitting similar to that seen for C_2H_6. Simulation of different antiphase domain superstructures suggests that the domains form superstructures of

$$\begin{vmatrix} 1 & 2 \\ 2 & 1 \end{vmatrix}$$

$$\begin{vmatrix} 1 & 2 \\ 3 & 0 \end{vmatrix}$$

and

$$\begin{vmatrix} 1 & 4 \\ 4 & 1 \end{vmatrix}$$

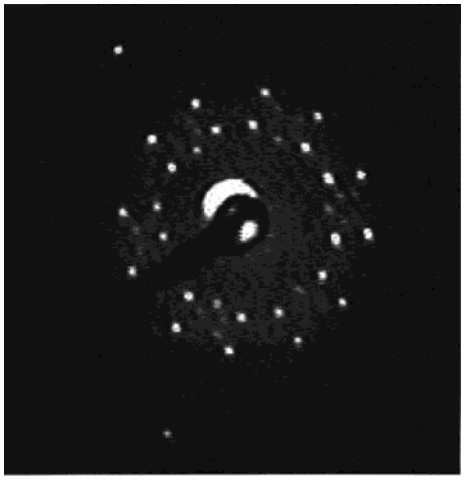

Figure 7. LEED image of Pt(111)−*n*-C_4H_{10} at a surface temperature of 100 K and a beam energy of 38 eV corresponding to the low-coverage structure where *n*-C_4H_{10} adsorbs parallel to the surface.

which are separated by the vectors $(l_1,l_2) = (1,2)$, (2,1), (3,0), (1,4), and (4,1). The p(2 × 2) structure for Pt(111)−C_3H_8 is shown in Figure 4c. The defective p(2 × 2) structure is in reasonable agreement with the coverage of 0.205 ML.

Pt(111)−*n*-C_4H_{10}. The clean surface was exposed to a background dose of *n*-butane at 3×10^{-8} Torr for 2 min 40 s at 100 K, annealed to 123 K, and subsequently quenched to 100 K in order to produce the LEED pattern shown in Figure 7, which we will refer to as the low-coverage (LC) *n*-butane structure. A similar pattern has been previously reported by Firment and Somorjai[44] at a beam energy of 19.5 eV; we used 38 eV to include the Pt(111) p(1 × 1) and show a larger section of the unit cell. We were not able to obtain a pattern while using such a low beam energy due to restrictions on the distance between the sample and the screen. Firment and Somorjai propose a real-space unit cell of

$$\begin{vmatrix} 2 & 1 \\ \bar{1} & 2 \end{vmatrix}$$

based on the van der Waals radius of *n*-butane. Our reciprocal space pattern is different and may be the result of differences in multiple scattering at the higher electron kinetic energy and/or different antiphase domain boundary-induced splitting. At this point, we cannot assign a structure to this LEED pattern, but we note that it does have a long-range order that is different from the high-coverage structure.

The clean surface was exposed to a background dose of *n*-butane at 3×10^{-8} Torr for 2 min 40 s at 100 K in order to produce the LEED pattern shown in Figure 8, which we will refer to as the high-coverage (HC) *n*-butane structure. A similar structure was also reported by Firment and Somorjai,[44] who interpreted their results as a real-space unit cell of

$$\begin{vmatrix} 3 & \bar{2} \\ 2 & 5 \end{vmatrix}$$

Both the LC and HC structures of butane exhibit overall hexagonal symmetry with subsymmetry in each hexagonal group, suggestive of scattering from multiple centers or antiphase domain splitting. The real-space structure of Pt(111)−*n*-C_4H_{10} proposed by Firment and Somorjai[44] is shown in Figure 4d.

Initial Trapping Probability. Initial trapping probability measurements for methane and ethane on each alkane precov-

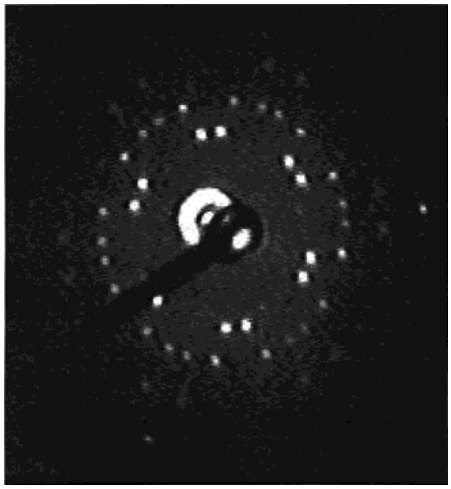

Figure 8. LEED image of Pt(111)−*n*-C_4H_{10} at a surface temperature of 100 K and a beam energy of 38 eV corresponding to the high-coverage structure.

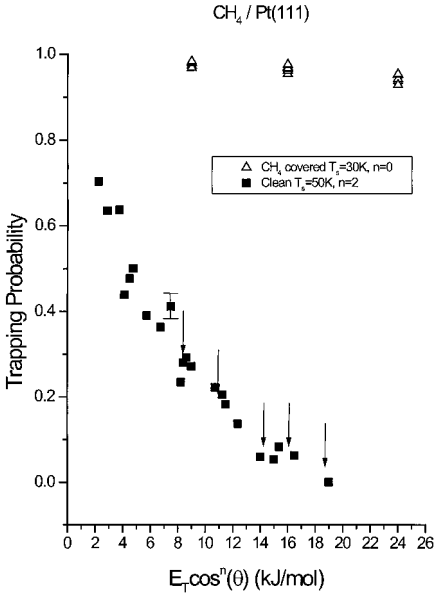

Figure 9. CH4 trapping probability on the clean (■) and CH_4-covered (Δ) surfaces at 50 and 30 K as a function of scaled incident energy. Points at normal incidence are marked with arrows for CH_4 trapping on the clean surface.

ered surface will be presented separately. Although some comparison will be made between the different surfaces, the bulk of the interpretation is found in the Discussion section of the paper. The empirical scaling relationship $E_T \cos^n(\theta)$ is used to best collapse the energy and angular dependencies of the trapping probability together into one curve where E_T is the incident kinetic energy of the molecule far from the surface and θ is the angle of approach measured with respect to the surface normal.

CH_4/Pt(111)−CH_4. The trapping probability of methane on the methane-covered surface at 30 K is shown as a function of incident energy and angle in Figure 9; for comparison, trapping probabilities for methane on the clean surface[1] are also shown. The trapping probability of methane on the methane layer is close to unity for energies between 9 and 24 kJ/mol, where the trapping probability of methane incident on the clean Pt(111) surface[1] is between 0.35 and 0. Methane trapping is greatly facilitated by the first layer of methane on the surface and shows no dependence on incident energy within experimental error; in contrast, on the clean surface, a strong energy dependence is

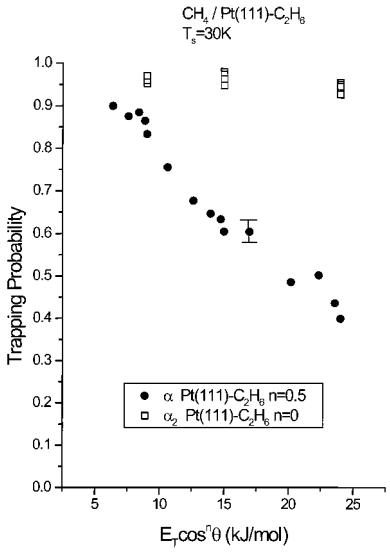

Figure 10. CH_4 trapping probability on the C_2H_6 (●) and combined $C_2H_6 + CH_4$ (□) adsorbate layers on Pt(111) as a function of the scaled incident energy at a surface temperature of 30 K.

exhibited.[1] In addition, methane trapping on the methane-precovered surface is independent of the incident angle, whereas methane trapping on the clean surface scales as $E_T \cos^2 \theta$. Methane molecules trapping on the clean surface feel a relatively smooth gas−surface potential, whereas molecules trapping onto a presaturated layer of methane at 30 K feel a more corrugated gas−surface potential, which manifests itself in total energy scaling of the trapping probability.

CH_4/Pt(111)−C_2H_6. The initial trapping probability of methane incident upon the ethane-covered surface at 30 K as a function of incident energy and angle is shown in Figure 10. The initial trapping probability, α, is greatly facilitated by preadsorbed ethane and shows a weaker dependence on energy than is observed on the clean surface. The trapping probability is only modestly dependent on the incident angle and scales with $E_T \cos^{0.5} \theta$, indicative of a more corrugated gas−surface potential than the clean surface. The initial trapping probability decreases from $\alpha = 0.9$ to 0.4 over the scaled energy range of 8 to 24 kJ/mol. At a given incident energy and angle, the adsorption probability on the ordered structure of ethane (0.227 ML) is significantly lower than that observed on a similarly ordered coverage of methane (0.237 ML).

Once the ethane-covered surface has adsorbed methane from the beam, the trapping probability α_2 remains constant, even as multilayers are formed. The trapping probability onto the combined ethane and methane layer is very high ($\alpha_2 \approx 0.96$) for all incident energies studied, and it is independent of the incident angle. Comparison of the DTPE at 50 K with that performed at 30 K (Figure 11) shows that multilayers of methane build on the surface at 30 K, but at 50 K, methane cannot form multilayers. The fact that the apparent trapping probability on the C_2H_6 presaturated surface at 50 K is 8% lower than that observed at 30 K is most probably the result of the competitive desorption of methane from the extrinsic precursor state at 50 K near saturation.[1]

CH_4/Pt(111)−C_3H_8. The initial trapping probability of methane incident on the structured propane overlayer at 30 K is shown as a function of incident energy and angle in Figure 12. Like methane trapping on methane- and ethane-covered surfaces, trapping is facilitated by the propane-covered surface and shows a weaker angular dependence than that on the clean surface. The initial trapping probability, α, is weakly dependent

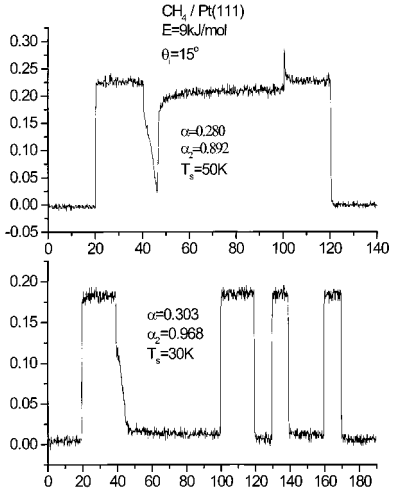

Figure 11. Dynamic trapping probability experiments (DTPEs) for CH_4 trapping on clean Pt(111) at 50 and 30 K; a second layer is not stable above 35 K.

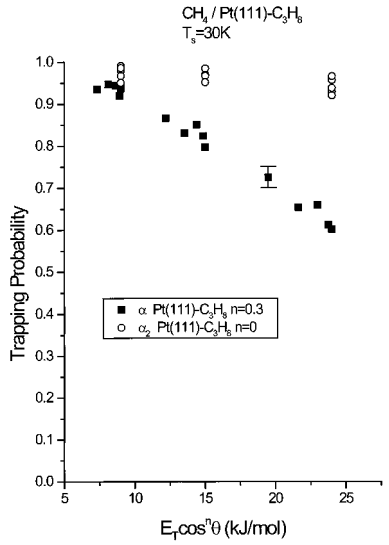

Figure 12. CH_4 trapping probability on the C_3H_8 (■) and combined $C_3H_8 + CH_4$ (○) adsorbate layers on Pt(111) as a function of the scaled incident energy at a surface temperature of 30 K.

on incident angle and scales with $E_T \cos^{0.3} \theta$, indicative of a more corrugated gas−surface potential than the clean surface ($E_T \cos^2 \theta$). The initial trapping probability decreases from 0.95 to 0.6 over the scaled energy range of 8 to 24 kJ/mol. The initial trapping probability of methane on the propane-covered surface (Figure 12) shows a dependence on energy and angle that is qualitatively similar to that observed on ethane (Figure 10), but trapping on the propane-covered surface is slightly more probable at all incident energies.

The trapping probability increases as the methane uptake increases until a constant value, α_2, is reached (0.96) for all incident energies studied, independent of incident angle. We conclude that multilayers of methane form on the surface, since at a surface temperature of 50 K the surface saturates with methane and the net adsorption probability falls to zero (Figure 11). The trapping probability onto the combined methane and propane layer at 30 K remains constant as multilayers of methane form, in exactly the same fashion as methane behaves when trapping on a methane or ethane/methane layer.

CH_4/Pt(111)−*n*-C_4H_{10}. The initial trapping probability of methane incident on the ordered low-coverage structure of *n*-butane (0.14 ML) at 40 and 31 K is shown as a function of

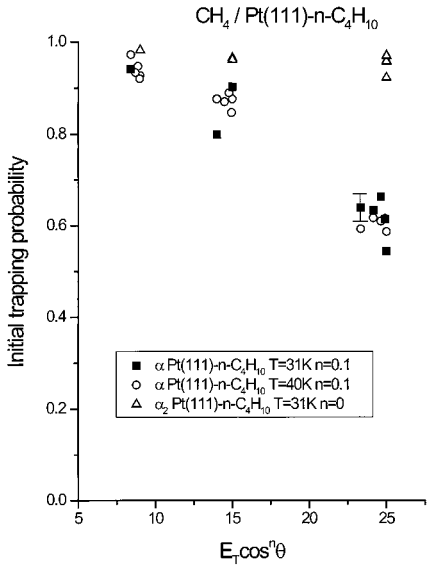

Figure 13. CH_4 trapping probability on the low-coverage C_4H_{10} (■) and combined $C_4H_{10} + CH_4$ (Δ) adsorbate layers on Pt(111) as a function of the scaled incident energy at a surface temperature of 30 K; the trapping probability of CH_4 on the *n*-C_4H_{10}-covered surface is the same at 40 K (○) as it is at 30 K.

incident energy and angle in Figure 13. The low-coverage structure of *n*-butane is believed to consist of *n*-butane adsorbed with its principal axis parallel to the surface.[44,57,63] Initial trapping (α) on the butane-covered surface exhibits an energy scaling of $E_T \cos^{0.1} \theta$, indicative of a gas−surface potential which is somewhat more corrugated than the ethane or propane-covered surfaces and significantly more corrugated than the clean surface. Data were taken at 40 K, where a second layer or multilayers are not stable, and at 31 K, where they are stable, to compare the initial trapping probabilities. The trapping probabilities and energy scaling are the same at 40 and 31 K, indicating that even if a second layer is stable, methane preferentially traps into vacancies in the first layer of *n*-butane on the surface until those states are filled. This result leads us to believe that methane will also complete the monolayer on the ordered structures of ethane and propane before forming multilayers and that methane is mobile on top of the adsorbed alkanes at 30 K. On this butane-covered surface, the initial trapping probability decreases from 0.94 to 0.55 in the scaled energy range of 8 to 25 kJ/mol. After the butane-covered surface has become covered at 31 K with methane from the beam, the trapping probability remains constant as multilayers accumulate. The trapping probability onto the combined butane and methane layer is very high (0.96) for all incident energies studied, independent of incident angle, as methane forms multilayers on top of the butane layer.

The initial trapping probability of methane incident on the high-coverage ordered structure of *n*-butane (0.20 ML) at 30 K as a function of incident energy and angle is shown in Figure 14. At this coverage, *n*-butane is believed to tilt upward from the surface.[44,57] The scaling exponent of 0.5 is indeed indicative of a gas−surface potential which is more corrugated than the clean surface ($n = 2$) but less corrugated than the low-coverage butane-covered surface ($n = 0.1$). At high coverage, the initial trapping probability decreases from $\alpha = 0.96$ to 0.65 in range of energy between 7 and 20 kJ/mol. After the high-coverage butane-covered surface becomes covered with methane at 30 K, the trapping probability remains constant as multilayers accumulate. The trapping probability onto the mixed butane−

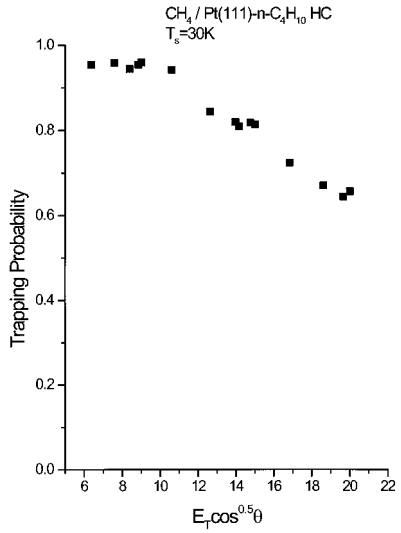

Figure 14. Methane trapping probability on the high-coverage structure of n-C_4H_{10} on Pt(111) at 30 K as a function of scaled incident energy.

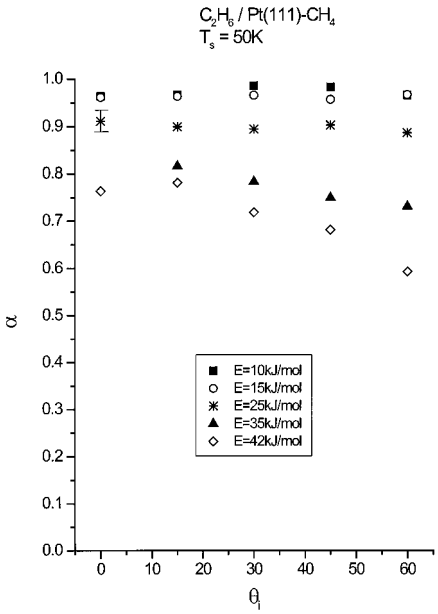

Figure 15. C_2H_6 trapping probability on CH_4-covered Pt(111) as a function of incident angle for differenct incident energies at a surface temperature of 50 K. As the incident energy is increased, the trapping probability begins to decrease with increasing incident angle.

methane layer is very high ($\alpha_2 \approx 0.96$) for all incident energies studied, independent of incident angle, even as methane forms multilayers.

C_2H_6/Pt(111)−CH_4. The initial trapping probability of ethane incident on the methane-covered surface at 50 K is shown as a function of incident energy and angle in Figure 15.[10] At low incident energies, the initial trapping probability is near unity, and there is no angular dependence, whereas at high incident energies, the initial trapping probability decreases with increasing incident angle ("negative" energy scaling), in contrast to what is usually observed for alkane trapping on clean[10,66] or covered[67] surfaces. Superposed on this unusual angular dependence is the usual energy dependence; the trapping probability decreases with increasing incident energy from 0.96 to 0.76 in the energy range of 10 to 42 kJ/mol at normal incidence. Ethane trapping on the methane-covered surface is the only case we have studied in which the binding energy and mass of the incident molecule are greater than those of the adsorbate molecule; either of these factors may contribute to the observed

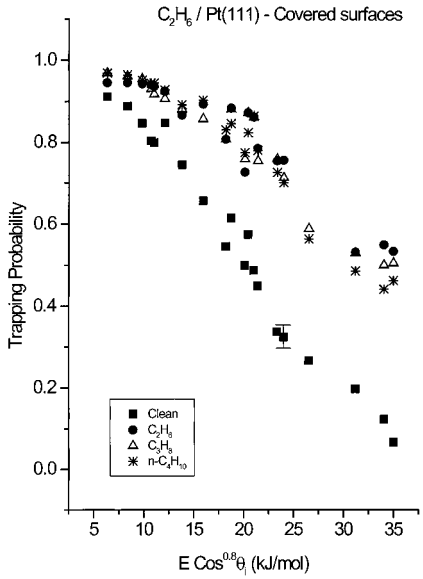

Figure 16. C_2H_6 trapping probability on C_2H_6 (●)-, C_3H_8 (Δ)-, and n-C_4H_{10} (*)-covered Pt(111) at a surface temperature of 50 K in contrast to the C_2H_6 trapping probability on the clean surface (■) at 95 K as a function of scaled incident energy.

negative energy scaling. During the DTPE of ethane, a very small amount of methane desorption was detected (∼1/10000 of the ethane adsorbed); only a very small amount of methane was displaced as a result of ethane adsorption. No desorption of the adsorbate molecules was detected for the other systems studied. Further spectroscopic studies are required to determine whether these adsorbates phase-separate. After the methane-covered surface has become covered with ethane from the beam, the trapping probability, α_2, remains constant as multilayers are formed. The trapping probability onto the combined ethane and methane layer is very high (∼0.96) for all incident energies studied, independent of incident angle, as ethane forms multilayers on top of the methane layer.

C_2H_6/Pt(111)−C_2H_6, C_3H_8, and n-C_4H_{10}. The initial trapping probabilities of ethane incident on ethane, propane, and low-coverage n-butane-covered surfaces at 50 K are shown as a function of incident energy and angle in Figure 16, along with the trapping probability of ethane on the clean surface at 95 K for comparison. Ethane trapping is facilitated on each of the covered surfaces and exhibits a scaling parameter indicative of a corrugated gas−surface potential. On the clean surface, the initial trapping probability decreases from 0.95 to 0.05 as the scaled incident energy is increased from 6 to 35 kJ/mol. In contrast, the initial trapping probability on each of the covered surfaces almost collapses onto a single curve with the appropriate energy scalings and decreases from 0.98 to 0.50 as the scaled incident energy is increased from 6 to 35 kJ/mol. Thus, each of the alkane-covered surfaces facilitates trapping, with only slightly different dynamical properties.

After each adsorbate-covered surface has become covered with ethane from the beam, the trapping probability remains constant at 0.96 as multilayers form for all incident energies studied, independent of incident angle. The energy scaling increases from 0.4 to 0.6 to 0.7 as the alkane chain length increases from ethane to propane to n-butane, suggesting that the gas−surface potential becomes smoother with increasing alkane chain length; only at the highest kinetic energies is a discernible difference in angular dependence detected (Figure 17). Recall that the coverage of each of these alkanes is as follows: methane (0.237 ML = 0.237 C/Pt), ethane (0.227 ML

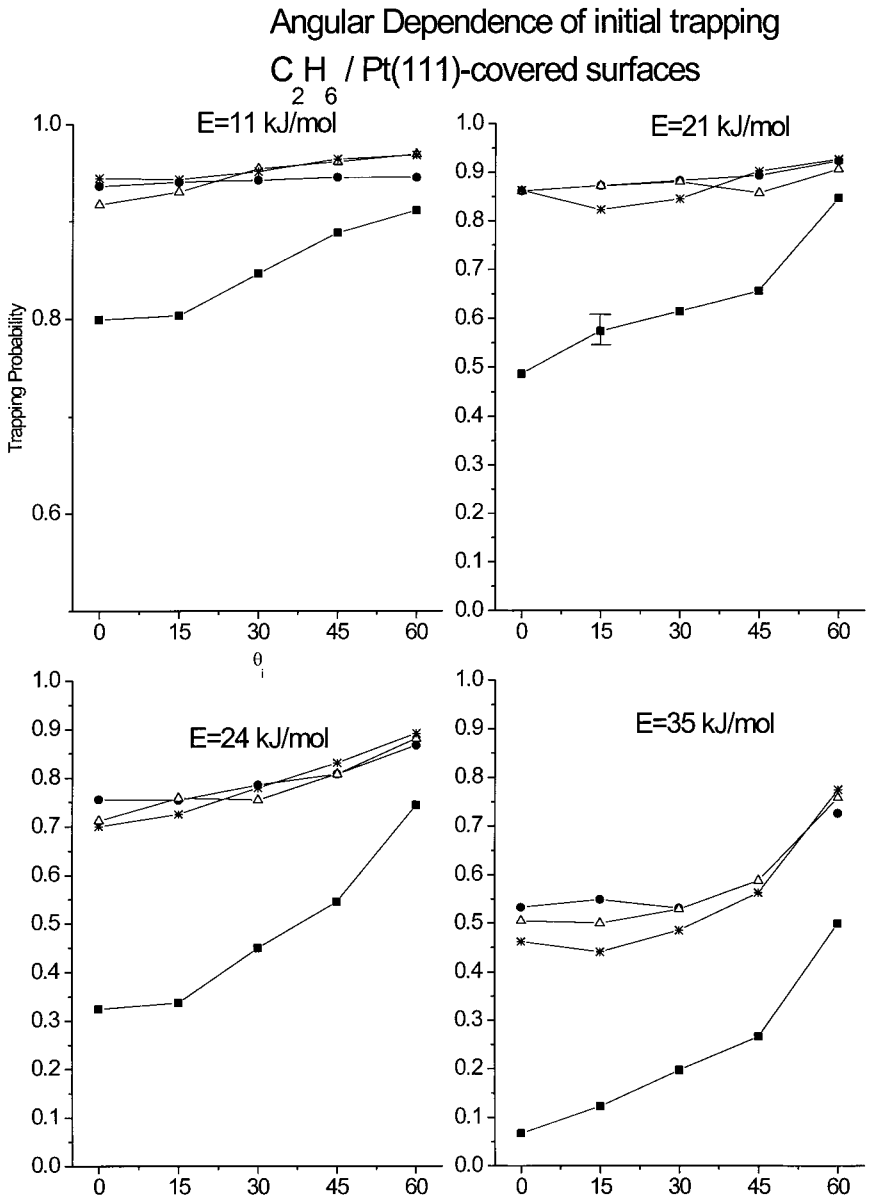

Figure 17. Angular dependence of C_2H_6 trapping on clean (■) and C_2H_6 (●)-, C_3H_8 (Δ)-, and *n*-C_4H_{10} (*)-covered Pt(111) at incident energies of 11, 21, 24, and 35 kJ/mol. At higher energies, slight differences in the angular dependence become more apparent.

= 0.45 C/Pt), propane (0.205 ML = 0.61 C/Pt), and the low-coverage structure of *n*-butane (0.14 ML = 0.56 C/Pt).[57] With an increasing number of C atoms per Pt atom, the ethane−surface potential appears to become slightly smoother, and the angular dependence of molecular trapping becomes somewhat more pronounced. This behavior is opposite that observed for methane; in effect, the larger size of ethane may average out the potential corrugation experienced by methane.

Discussion

Coverage Dependence of Trapping Probability. Even after the surface has been presaturated with a single layer of alkane from the background or the dose from the beam, the trapping probability continues to increase as the surface becomes further covered with the incident alkane. At 30 and 50 K, methane and ethane are clearly stable in multilayers because the trapping probability remains near unity as adsorption continues indefinitely. Trapping on top of the second layer is even more efficient than trapping onto the first. During trapping into the structured alkane layer initially present, the DTPE curve is convex upward, indicating an increase in the trapping probability of the incident molecule with increasing coverage. Such behavior has been modeled previously for ethane,[41] methane,[1] and argon[42] molecular molecular adsorption into the monolayer on clean Pt(111) using the modified Kisliuk model described above. In the case of trapping on a surface with submonolayer coverage, there is a clear distinction between collisions with bare surface regions and the adsorbed species. After the first layer has been filled, it is possible that the same type of behavior exists once again for the second layer, wherein trapping is more efficient than trapping into the first layer. After the second layer has been filled, the trapping probability of methane and ethane on all the alkane-covered surfaces is near unity, and no further change in the trapping behavior is detected, indicating that trapping into the third and subsequent layers is the same.

Enhanced Trapping Probability. The trapping probability of methane varies somewhat systematically with the nature of adsorbate covering the surface. Generally, except for preadsorbed methane, the trapping probability increases as the molecular weight of the preadsorbed alkane increases (Figure

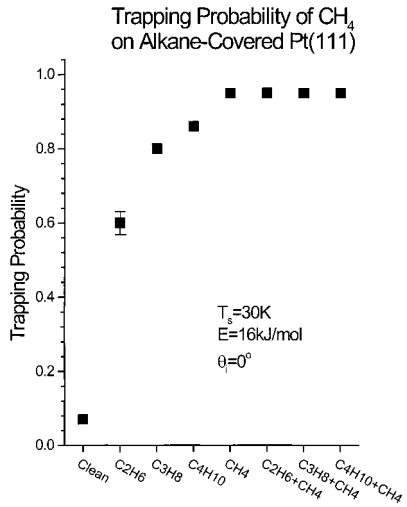

Figure 18. CH_4 trapping probability as a function of adsorbate covering the Pt(111) surface at a normal incident energy of 16 kJ/mol and a surface temperature of 30 K. The methane trapping probability increases as the molecular weight and carbon coverage of the alkane on the surface increases, with the exception of the methane-covered surface.

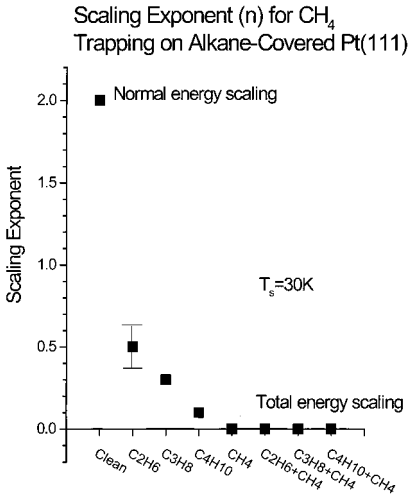

Figure 19. Energy-scaling exponent for CH_4 trapping as a function of adsorbate covering the Pt(111) surface; a higher energy-scaling exponent indicates a more pronounced angular dependence of the trapping probability.

18). For a given energy at normal incidence, the trapping probability on the clean surface is 0.07 and increases to 0.85 for adlayers of C_2-C_4 alkanes; the methane trapping probability onto the combined methane and alkane layers is consistently near unity. The scaling exponent observed is shown for each adsorbate covering the surface in Figure 19. A scaling exponent near 2 (normal energy scaling) indicates a strong angular dependence, whereas a scaling exponent of 0 indicates no angular dependence (total energy scaling). Though there is definitely some uncertainty in the determination of *n*, there is a clear trend of the scaling parameter with molecular weight for C_2-C_4 (Figure 20). The scaling exponent is 2 on the clean surface and decreases smoothly toward 0 as the molecular weight of the alkane is increased, with the exception of the methane-covered surface, which exhibits total energy scaling. The dynamics of ethane trapping are not sensitive enough to the type of adsorbate covering the surface to merit detailed attention.

A simple mechanism which could explain the enhanced trapping probability is translational energy transfer from the incident molecule to the adsorbate species. The modified Baule formula,[45,68] which uses a square well potential of depth *D*, an incident molecule energy E_T, an incident molecule of mass *m*, and a surface species of mass *M* gives the energy transfer in a collision Δ as

$$\Delta = \frac{4mM(E_T + D)}{(M + m)^2}$$

Approximating the surface mass of the adsorbed alkane, *M*, as a multiple of the mass of methane, *m* ($M = nm$), gives

$$\Delta = \frac{4n}{(n + 1)^2}(E_T + D)$$

which shows that as the disparity between the gas and surface masses increases, the energy loss in a collision decreases, albeit slowly. This mass effect predicts that incident molecules are less likely to trap on surfaces covered by weakly held adsorbates as *n* increases. Although this model shows some promise for argon trapping on Ar- and Xe-covered Pt(111), for methane trapping on the alkane-covered surfaces, the prediction is in direct disagreement with experiment, suggesting that differences in direct translational energy exchange are not the dominant source of differences in trapping probabilities and energy scaling, except perhaps on the methane-covered surface.

Methane and ethane trapping onto alkane-covered surfaces may also be facilitated by energy transfer to internal modes of the adsorbed molecules. Previous studies[66] have shown that the trapping of larger alkanes is facilitated by the conversion of translational energy to the rotational energy of the incoming gas-phase molecule, but since the adsorbed molecules are lying flat in an ordered structure and are relatively closely packed (particularly propane and *n*-butane), it is unlikely that free rotational excitation of adsorbed molecules is a viable energy sink. This could produce a near continuum of frustrated vibrations that may be involved in the process. Certainly, energy transfer to rotational modes cannot be responsible for the high efficiency of trapping produced by adsorbed methane.

The translational energy of the incident alkane may also be transferred to internal vibrations of the adsorbate molecules. C−C bonds (1000 cm^{-1}) of the adsorbed molecule have vibrational energies lower than those of C−H (3000 cm^{-1}) bonds, but they are not likely to be excited at the incident energies of methane and ethane used in this study.[69] Accordingly, simulations of C_3H_8 trapping on Pt(111) indicate that the C−C stretching (1000 cm^{-1}) and bending modes of propane are not excited,[70] and thus, such modes are not expected to be excited by the incident methane for the same incident energies here. Furthermore, facilitated trapping is observed at normal incidence, where the impinging molecules are impinging perpendicular to C−C bonds; in this collision configuration, excitation of the C−C bond is not likely. Furthermore, lower-frequency transverse modes, such as the torsional mode of *n*-butane, may be very difficult to excite because the molecule is adsorbed lying flat on the surface. Again, such modes clearly cannot contribute to enhanced trapping on the methane-covered surface. However, the details of these energy exchange processes await the results of more advanced molecular dynamics simulations.

The general enhancement in the trapping produced by these weakly held adlayers is consistent with direct energy exchange coupled with a change in the corrugation of the gas−surface potential. The enhancement in ethane trapping probability on a sulfur-covered Pt(111) surface[8] has been associated with an increased static corrugation in the gas−surface potential, which

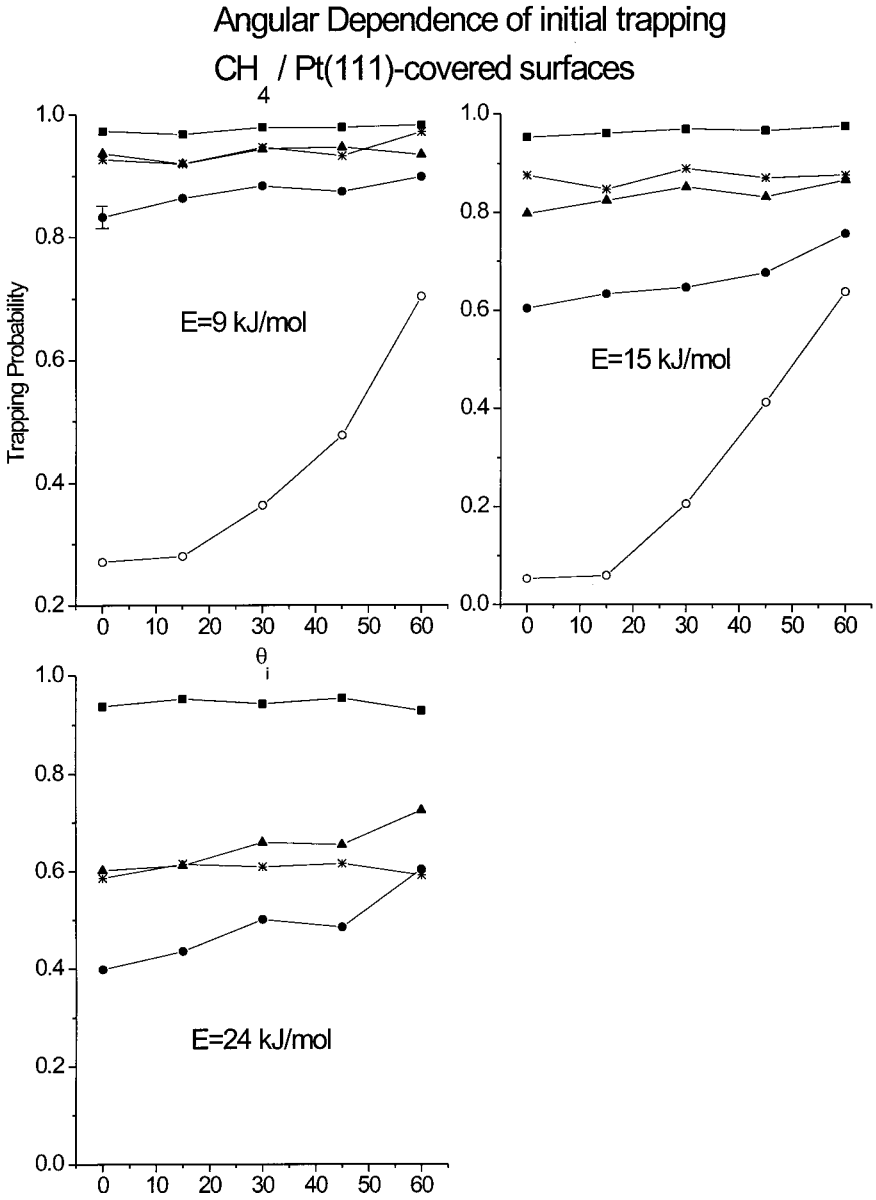

Figure 20. Angular dependence of CH_4 trapping on clean (○) and CH_4 (■)-, C_2H_6 (●)-, C_3H_8 (▲)-, and *n*-C_4H_{10} (*)-covered Pt(111) at incident energies of 9, 15, and 24 kJ/mol.

facilitates the interconversion of the perpendicular-to-parallel momentum.[67] The corrugation in the gas−surface potential affects the angular dependence of trapping; a more corrugated gas−surface potential results in total or near-total energy scaling ($n \approx 0.5-0.0$), whereas a smooth gas−surface potential results in normal energy scaling ($n \approx 2.0$). A clear correlation between the corrugation in the gas−surface potential and the trapping probability is shown in Figure 21; as the scaling exponent decreases from $n = 2$ on the smooth, clean surface to $n = 0$ on the corrugated, methane-covered surface, the trapping probability increases from 0.07 to 0.96.

The methane trapping probability on the methane-covered surface is greater than the trapping probability on the ethane-, propane-, and butane-covered surfaces. As discussed above, this result cannot be explained by the excitation of the vibrational or rotational modes. The total carbon coverage increases as the chain length of alkane adsorbate increases,[44] which in turn appears to produce an increased corrugation in the gas−surface potential for methane trapping. However, methane exhibits the lowest carbon coverage but, at the same time, the highest degree of trapping and surface corrugation. This anomaly in the otherwise logical progression suggests that the methane adlayer may deformable, lending a dynamic corrugation to the gas−surface potential in addition to the static corrugation observed for the ethane-, propane-, and butane-covered surfaces. A dynamic corrugation in the gas−surface potential has been observed in molecular dynamics simulations of Ar trapping on Ar-covered Ru(001) by Head-Gordon and Tully,[7] where Ar adsorbates are displaced slightly during a collision.

Angular Dependence of Trapping. Methane incident on an adsorbate-covered surface feels a much more corrugated gas−surface potential than it does during a collision on the clean surface. The energy-scaling exponent is 2 on the clean surface, 0.5 on ethane, 0.3 on propane, and 0.1 on *n*-butane, indicating an increasing degree of corrugation as the length of alkane (and the density of the adlayer) increases. Previous studies conducted above temperatures where a second layer is stable reveal that methane is able to adsorb onto the first layer of adsorbed alkane.[10] Furthermore, since the coverage (molecules/cm^2) of each of the alkanes is approximately the same,[10] the decrease in "bare" surface area seen by the incident methane molecules decreases with the increasing molecular weight of the hydro-

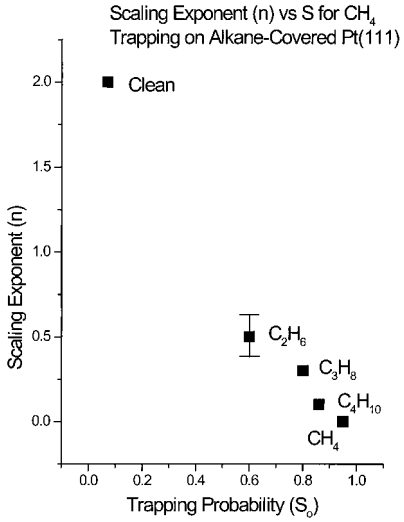

Figure 21. Correlation between the energy-scaling exponent and the trapping probability of CH_4 on various alkane-covered Pt(111) surfaces for a normal incident energy of 30 kJ/mol. As the corrugation in the gas−surface potential increases, the trapping probability increases.

carbon. Since bare surface regions show no corrugation for CH_4 trapping, the increase in the corrugation parameter, *n*, with the molecular weight of the alkane may simply be related to the decreasing "free" surface.

The scaling parameter for methane trapping is $n = 0.5$ on the high-coverage *n*-butane structure ($\theta = 0.20$ ML) and $n = 0.1$ on the low-coverage *n*-butane structure ($\theta = 0.14$ ML). The change in scaling parameter, indicative of the corrugation in the static gas−surface potential, may be indicative of different structures of these adlayers. The molecular dynamics simulations of Raut et al. [71] predict a flat-lying *n*-butane structure on Pt(111) at low coverages which tilts upward at an angle of 40−80° from the surface plane at high coverages. Methane trapping on the closely packed, tilted phase of *n*-butane apparently feels a less corrugated gas−surface potential.

Ethane trapping on the adsorbate-covered surfaces also feels a more corrugated gas−surface potential than it does on the clean surface, although the difference is not as pronounced as that for methane trapping. The energy-scaling exponent is 0.8 on the clean surface, 0.3 on ethane, 0.6 on propane, and 0.7 on *n*-butane. In contrast to methane trapping, previous studies conducted at 95 K, above which a second layer is stable[11] show no adsorption of ethane[10] into C_3H_8- and *n*-C_4H_{10}-covered surfaces. At 50 K, ethane probably adsorbs directly into the second layer, followed by multilayer growth. Since the surface area covered by alkane on the surface increases with increasing chain length, ethane may feel a less corrugated gas−surface potential because it is too large to sense corrugations accessible to methane.

Energy-scaling exponents of 0.6, 0.7, and 0.8 are actually within the experimental error in the scaling exponent, which we estimate to be ±0.15. Furthermore, the scaling function, $E_T \cos^n \theta$, is an empirical relationship with little theoretical validity. Another approach to showing the apparent gas−surface potential corrugation is to plot the trapping probability as a function of the incident angle for a given energy, as shown in Figure 17. At incident energies of 11, 21, and 24 kJ/mol, the ethane trapping probability onto each of the covered surfaces is near unity, with no clear distinction in the angular dependence on the different surfaces. At 35 kJ/mol, the ethane trapping probability onto the *n*-butane-covered surface shows an angular dependence slightly steeper than that from trapping onto the propane-covered surface, which in turn has a slightly steeper angular dependence than that from trapping onto the ethane-covered surface; the order of the energy-scaling exponents appears justified.

TABLE 1. Trapping Probabilities of Methane on Various Alkane-Covered Surfaces at Incident Energy *E* and Incident Angle θ at a Surface Temperature of 30 K[a]

E	θ	CH_4	C_2H_6	C_3H_8	LC *n*-C_4H_{10}	HC *n*-C_4H_{10}	clean
9	0	0.973	0.833	0.937	0.927	0.959	0.271
9	15	0.968	0.864	0.92	0.92	0.954	0.28
9	30	0.979	0.884	0.944	0.947	0.944	0.363
9	45	0.979	0.875	0.947	0.933	0.958	0.477
9	60	0.983	0.899	0.935	0.972	0.954	0.703
15	0	0.953	0.604	0.797	0.876	0.813	0.053
15	15	0.961	0.633	0.824	0.847	0.817	0.059
15	30	0.969	0.646	0.851	0.889	0.819	0.205
15	45	0.966	0.676	0.831	0.87	0.843	0.411
15	60	0.975	0.755	0.866	0.876	0.942	0.637
24	0	0.937	0.398	0.602	0.586		
24	15	0.952	0.435	0.612	0.615		
24	30	0.942	0.501	0.659	0.609		
24	45	0.953	0.485	0.654	0.616		
24	60	0.928	0.604	0.725	0.592		
20						0.656	
20						0.643	
20						0.67	
20						0.723	
20						0.809	

[a] Trapping probabilities of methane on the clean surface are for comparison.

Energy Dependence. The trapping probability of methane and ethane on all the alkane-covered surfaces decreases with increasing incident energy, as is expected for molecular adsorption.[72] However, the energy dependence is weak compared with that of the clean surface, as shown in Figure 9 for methane trapping on the clean surface compared with methane trapping on a methane-covered surface. Where the trapping probability decreases from 0.4 to 0 in the energy range of 10 kJ/mol $< E <$ 15 kJ/mol for the clean surface, it decreases only from 0.8 to 0.6 on the ethane-covered surface. Table 1 shows that the measured trapping probability of methane on the methane-covered surface is almost independent of incident energy and angle, suggestive of perfect mass matching. As discussed earlier, the enhancement of molecular trapping on the alkane-covered surface is most likely due to a more corrugated gas−surface potential. The effects of the potential of the alkane-covered surface are more pronounced at higher incident energies, where more energy must be dissipated in order for the incident molecule to trap. Table 1 shows that the trapping probability behavior of methane on each of the flat-lying alkane-covered surfaces is similar, as would be expected for the similar methyl−methyl potential that would be experienced in each of the cases. The similarity in the trapping behavior of ethane on each of the covered surfaces can be seen in Figure 16.

Conclusions

Methane and ethane trapping on Pt(111) at low temperature is enhanced compared to trapping on the clean surface at the same energies by adsorbed alkanes via trapping into an extrinsic precursor state. The enhancement is most likely due to energy transfer to the adsorbed species and appears to be strongly affected by an increase in the corrugation of the gas−surface potential. For methane, after the monolayer is filled, subsequent layers build with near-unit trapping probability regardless of the type of alkane in the first layer. The trapping probability for methane increases with increasing adsorbate chain length

and carbon coverage—the methane-precovered surface being an exception. The relative constancy of the trapping probability of methane on the methane-saturated surface with incident energy and angle suggests that mass matching plays an important role in the methane−methane trapping interaction. The angular dependence of the initial trapping probability for methane on the covered surfaces indicates an increasing corrugation in the gas−surface potential with increasing chain length of adsorbate, which in turn implies that higher carbon atom coverage leads to a more corrugated gas−surface potential for methane, since the absolute coverage of each of the alkanes is about the same.[10] Ethane trapping onto the second layer is enhanced to approximately the same degree on all the covered surfaces.

References and Notes

(1) Carlsson, A. F.; Madix, R. J. *Surf. Sci.* **2000**, *458*, 91.
(2) Weinberg, W. H. In *Dynamics of Gas-Surface Interactions*; Rettner, C. T., Ashfold, M. N. K., Eds.; Royal Society of Chemistry: London, 1991; p 171−216.
(3) D'Evelyn, M. P.; Madix, R. J. *Surf. Sci. Rep.* **1984**, *4*, 1.
(4) Barker, J. A.; Auerbach, D. J. *Surf. Sci. Rep.* **1985**, *4*, 1.
(5) Arumainayagam, C. R.; Madix, R. J. *Prog. Surf. Sc.* **1991**, *38*, 1.
(6) Lombardo, S. J.; Bell, A. T. *Surf. Sci. Rep.* **1991**, *13*, 1.
(7) Head-Gordon, M.; Tully, J. C. *Surf. Sci.* **1992**, *268*, 113.
(8) Stinnett, J. A.; McMaster, M. C.; Madix, R. J. *Surf. Sci.* **1996**, *364*, 325.
(9) Kao, C. L.; Carlsson, A. F.; Madix, R. J. Manuscript in preparation.
(10) Carlsson, A. F.; Madix, R. J. Manuscript in preparation.
(11) Carlsson, A. F.; Madix, R. J. *To be published* **2000**.
(12) Weinberg, W. H. *Kinetics of Interface Reactions*; Springer: New York, 1986.
(13) Kreuzer, H. J.; Gortel, Z. W. *Physisorption Kinetics*; Springer: New York, 1986.
(14) Gomer, R. *Discuss. Faraday Soc.* **1959**, *28*, 23.
(15) Hofmann, P.; Horn, K.; Bradshaw, A. M.; Jacobi, K. *Surf. Sci.* **1979**, *82*, L610.
(16) Opila, R.; Gomer, R. *Surf. Sci.* **1981**, *105*, 41.
(17) Hsu, Y. P.; Jacobi, K.; Rotermund, H. H. *Surf. Sci.* **1982**, *117*, 581.
(18) Grunze, M. J.; Fuhler, J.; Neumann, M.; Brundle, C. R.; Auerbach, D. J.; Behm, R. J. *Surf. Sci.* **1984**, *139*, 109.
(19) Engel, T. *J. Chem. Phys.* **1978**, *69*, 373.
(20) Campell, C. T.; Ertl, G.; Kuipers, H.; Senger, J. *Surf. Sci.* **1981**, *107*, 207.
(21) Campell, C. T.; Ertl, G.; Senger, J. *Surf. Sci.* **1982**, *115*, 309.
(22) Senger, J.; Robota, H.; Vielhaber, W.; Ertl, G.; F. F.; Hager, J.; Krieger, W.; Walther, H. *Surf. Sci.* **1983**, *131*, 273.
(23) Mitchell, W. J.; Xie, J.; Lyons, K. J.; Weinberg, W. H. *J. Vac. Sci. Technol., A* **1994**, *12*, 2250.
(24) Lutsishin, P. P.; Panchenko, O. A.; Shpagin, V. F. *Surf. Sci.* **1992**, *278*, 218.
(25) Heidberg, J.; Hussla, I. *Vibrations at Surfaces*; Plenum: New York, 1980.
(26) Lauterbach, J.; Sushchikh, M.; Weinberg, W. H. *Z. Phys. Chem.* **1997**, *198*, 99.
(27) Sjovall, P.; Uvdal, a. P. *J. Vac. Sci. Technol.* **1998**, *16*, 943.
(28) Bradley, J. M.; Guo, X.-C.; Hopkinson, A.; King, D. A. *J. Chem. Phys.* **1996**, *104*, 4283.
(29) Bradley, J. M.; Hopkinson, A.; King, D. A. *Surf. Sci.* **1997**, *371*, 255.
(30) Arumainayagam, C. R.; McMaster, M. C.; Madix, R. J. *Surf. Sci.* **1990**, *237*, L424.
(31) Arumainayagam, C. R.; McMaster, M. C.; Madix, R. J. *J. Vac. Sci. Technol. A* **1991**, *9*, 1581.
(32) Hamza, A. V.; Ferm, P. M.; Budde, F.; Ertl, G. *Surf. Sci.* **1988**, *199*, 13.
(33) Haase, G.; Asscher, M. *Surf. Sci.* **1987**, *191*, 75.
(34) Guo, X. C.; Bradley, J. M.; Hopkinson, A.; King, D. A. *Surf. Sci.* **1994**, *310*, 163.
(35) Beutl, M.; Rendulic, K. D.; Castro, G. R. *Surf. Sci.* **1997**, *385*, 97.
(36) Hopkinson, A.; Guo, X.-C.; Bradley, J. M.; D. A. King *J. Chem. Phys.* **1993**, *99*, 8262.
(37) Hodgson, A.; Lewin, A. K.; Nesbitt, A. *Surf. Sci.* **1993**, *293*, 211.
(38) Grimblot, J. *J. Electron Spectrosc. Relat. Phenom.* **1990**, *52*, 161.
(39) Luntz, A. C.; Grimblot, J.; Fowler, D. E. *Phys. Rev. B* **1989**, *39*, 12903.
(40) Prince, K. C.; Paolucci, G.; Bradshaw, A. M. *Surf. Sci.* **1986**, *175*, 101.
(41) Arumainayagam, C. R.; McMaster, M. C.; Madix, R. J. *J. Phys. Chem.* **1991**, *95*, 2461.
(42) Carlsson, A. F.; Madix, R. J. Manuscript in preparation.
(43) Kang, H. C.; Mullins, C. B.; Weinberg, W. H. *J. Chem. Phys.* **1990**, *92*, 1397.
(44) Firment, L. E.; Somorjai, G. A. *J. Chem. Phys.* **1977**, *66*, 1901.
(45) Persson, M.; Harris, a. J. *Surf. Sci.* **1987**, *187*, 67.
(46) Logan, R. M.; Stickney, R. E. *J. Chem. Phys.* **1966**, *44*, 195.
(47) Logan, R. M.; Keck, J. C. *J. Chem. Phys.* **1968**, *49*, 860.
(48) Nichols, W. L.; Weare, J. H. *J. Chem. Phys.* **1975**, *62*, 3754.
(49) Tully, J. C. *J. Chem. Phys.* **1990**, *92*, 680.
(50) D'Evelyn, M. P.; Hamza, A. V.; Gdowski, G. E.; Madix, R. J. *Surf. Sci.* **1986**, *167*, 451.
(51) Feulner, P.; Menzel, a. D. J. *J. Vac. Sci. Technol.* **1980**, *17*, 662.
(52) Feulner, P.; Menzel, D. J. *Surf. Sci.* **1985**, *154*, 465.
(53) Schlichting, H.; Menzel, D. *Rev. Sci. Instrum.* **1993**, *64*, 2013.
(54) King, D. A.; Wells, M. G. *Surf. Sci.* **1972**, *29*, 454.
(55) D'Evelyn, M. P.; Steinruck, H. P.; Madix, R. J. *Surf. Sci.* **1987**, *180*, 47.
(56) Yates, J. T. *Experimental Innovations in Surface Science: A Guide to Practical Laboratory Methods and Instruments*; Springer: New York, 1998.
(57) Weaver, J. F.; Ikai, M.; Carlsson, A. F.; Madix, a. R. J. *T*Manuscript in preparation.
(58) Norton, P. R.; Davies, J. A.; Jackman, T. E. *Surf. Sci.* **1982**, *122*, L593.
(59) Td, CH_4, multilayer = 35 K; Td, CH_4, monolayer = 67 K; Td, C_2H_6, multilayer = 65 K; Td, C_2H_6, monolayer = 120 K. Carlsson, A. F.; Madix, R. J. Unpublished Data, 2000.
(60) Ellis, W. P. In *Optical Transforms*; Lipson, H., Ed.; Academic Press: London, 1972; p 253.
(61) Ertl, G.; Kuppers, J. *Low Energy Electrons and Surface Chemistry*; Verlag Chemie: Berlin, 1974.
(62) Bocquet, B.; Gauthier, S. *Surf. Sci.* **1998**, *416*, 1.
(63) Duszak, R.; Prince, R. H. *Surf. Sci.* **1990**, *226*, 33.
(64) Horiguchi, T.; Nakanishi, S. *Acta Crystallogr., Sect. A* **1975**, s288.
(65) VanHove, M. A.,.
(66) Weaver, J. F. Doctoral Thesis, Stanford University, Stanford, CA, 1998.
(67) Stinnett, J. A.; Weaver, J. F.; Madix, R. J. *Surf. Sci.* **1998**, *395*, 148.
(68) Weinberg, W. H.; Merrill, R. P. *J. Vac. Sci. Technol.* **1971**, *8*, 718.
(69) Arumainayagam, C. R.; Schoofs, G. R.; McMaster, M. C.; Madix, R. J. *J. Phys. Chem.* **1991**, *95*, 1041.
(70) Stinnett, J. A.; Madix, R. J. *J. Chem. Phys.* **1996**, *105*, 1609.
(71) Raut, J. S.; Scholl, D. S.; Fichthorn, K. A. *Surf. Sci.* **1997**, *389*, 88.
(72) Harris, J. In *Dynamics of Gas-Surface Interactions*; Rettner, C. T., Ashfold, M. N. R., Eds.; Royal Society of Chemistry: London, 1991; p 3.